Optical and Quantum Electronics (2020) 52:279
https://doi.org/10.1007/s11082-020-02407-4

The impact of the carrier concentration and recombination current on the p^+pn CZTS thin film solar cells

Shahin Enayati Maklavani[1] · **Shahram Mohammadnejad**[1]

Received: 2 February 2020 / Accepted: 13 May 2020 / Published online: 20 May 2020

Abstract
One of the main causes of low performance of Cu_2ZnSnS_4 (CZTS) based thin film solar cells is its high recombination current. In this paper, the effects of the carrier concentration and recombination current in the CZTS thin film solar cells have been carefully scrutinized. In continue, for comparison and validation, two simulated structures based on the CZTS absorber layer have been reproduced and the influence of the absorber layer defects and carrier concentration has been analyzed. In this work, two different structures using p^+-CZTS intermediate layer (between the CZTS absorber layer and Mo back-contact) and dual CZTS layer have been proposed and optimized to decrease recombination and extract the desired photovoltaic parameters. By using and optimizing these structures as p^+pn junction, 15.62% and 19.08% efficiencies have been achieved in p^+-CZTS intermediate layer and p^+pn CZTS dual layer structures, respectively. The highest efficiency of dual absorber based solar cell is achieved when the carrier concentration of the p^+-CZTS and p-CZTS absorber layers is 1×10^{18} cm^{-3} and 5×10^{15} cm^{-3}, respectively. Moreover, the optimum thickness of the p^+-CZTS and p-CZTS absorber layers in p^+pn CZTS dual layer structure is 1 and 1.5 μm, respectively. Finally, the total recombination current density is reduced to 2.05 mA/cm^2.

Keywords CZTS solar cell · Recombination current · p^+pn structure · Carrier concentration · Efficiency

1 Introduction

Photovoltaic Solar energy is the most renewable, reliable, and accessible energy in the world. One hour of solar radiation provides the amount of energy needed in one year (Rizi et al. 2018). High efficiency, cheap production and long durability are the advantages of photovoltaic technology (Pawar et al. 2010; Maklavani and Mohammadnejad 2020). The large number of photovoltaic cells in the market is first-generation solar cells that use high-thickness silicon semiconductors. Despite rich silicon resources, there is no possibility of

✉ Shahram Mohammadnejad
Shahramm@iust.ac.ir

[1] Department of Electrical Engineering, Iran University of Science and Technology, P.O. Box: 1684613114, Tehran, Iran

further increase the conversion efficiency of silicon based solar cells due to lower silicon absorption. Therefore, high-absorption materials instead of silicon have been studied as second-generation thin film solar cells. These include cadmium telluride (CdTe), copper indium selenide (CIS), copper indium gallium selenide (CIGS) and copper zinc tin sulfide (CZTS) (Hossain 2012; Guo et al. 2018). Although CdTe, CIS, and CIGS are currently industrialized, the indium, cadmium and tellurium in these materials are rare and toxic elements (Guo et al. 2018; Dey et al. 2017).

The kesterite structure of the CZTS has a direct bandgap energy of about 1.5 eV and high absorption coefficient above 10^4 cm^{-1} (Adewoyin et al. 2017a), which is similar to CIGS. As a result, CZTS semiconductors are potential substitutes for CIGS. All components of the CZTS are non-toxic and earth abundant. Thus, in comparison with CIGS, the use of various earth-abundant kesterite materials has enhanced (Adewoyin et al. 2019). Therefore, CZTS is expanding as a photovoltaic material due to the high quality, high absorption and low cost (Ramanujam et al. 2016; Pal et al. 2019).

In 2013, Shin et al. fabricated CZTS solar cells with efficiency of 8.4% (Shin et al. 2013). Structure of the cell is Mo/CZTS/CdS/i-ZnO/ZnO:Al and was a record efficiency for several years. This basic structure is similar to the basic structure of other thin film solar cells based on CIGS and CdTe (Bahrami et al. 2013). One way to improve the absorber/buffer interface and reduce the recombination current is changing the buffer layer or using a hybrid buffer (Khoshsirat and Yunus 2016; Neuschitzer et al. 2016; Yan et al. 2016; Cherouana and Labbani 2017; Wanda et al. 2019). The efficiency of 9.2% has been reported by using $Zn_{1-x}Cd_xS$ as the buffer layer in CZTS based solar cells (Sun et al. 2016). In 2018, the 11% efficiency (as a highest efficiency) of CZTS solar cell was applied by adding a ultrathin layer of Al_2O_3 on the back of the CZTS absorber to improve band alignment in Mo contact/CZTS absorber interface (Yan et al. 2018). This structure reduces the thickness of the MoS_2 layer and decreases the degradation of CZTS in this area. However, the Al_2O_3 and CZTS lattice constants are 4.16 Å (Degen et al. 2005) and 5.45 Å (Nagaoka et al. 2014), respectively which have highly mismatched. Moreover, $Cu_2ZnSn(S,Se)_4$ is formed by adding selenium to CZTS. As selenium increases, the bandgap of the CZTSSe changes from 1.5 to 1 eV. The CZTSSe based solar cells have higher efficiency and short circuit current. But, they have a lower open circuit voltage. The highest efficiency of 12.6% has been reported by CZTSSe based solar cells (Wang et al. 2014).

Anyway, the maximum efficiency of CZTS solar cells is about half of the highest efficiency of CIGS and CdTe solar cells. The maximum efficiency of CIGS and CdTe solar cells is 23.35% (Nakamura et al. 2019), and 22.1% (Green et al. 2019), respectively. In addition, the high efficiency for the CZTS cell is one-third of the Shockley-Queisser limit (32.2%) (Adewoyin et al. 2017a; Seol et al. 2003; Wang et al. 2014). Hence, it is very important to design and fabricate high-efficiency CZTS based solar cells. Variety factors have affected reduction performance including a lot of defects related to band tailing (Miller et al. 2012; Shin et al. 2017), a thick unwanted MoS_2 layer at the Mo/CZTS interface (Scragg et al. 2013), the existence of secondary phases (Scragg et al. 2013; Siebentritt 2013), and undesirable band offset at back-contact/CZTS and CZTS/CdS interface (Crovetto and Hansen 2017) (Yan et al. 2018). These factors cause severe non-radiative recombination and thus decrease the whole performance of CZTS thin film solar cells (Yan et al. 2018).

Various designs of the CZTS solar cells have been proposed such as bandgap grading (Yang et al. 2016; Mohammadnejad and Parashkouh 2017), buffer layer changing (Pandey and Mukherjee 2013; Wanda et al. 2019) and optimization of some device parameters (Adewoyin et al. 2017b; Patel and Ray 2012). Nonetheless, there is no significant

enlargement in experimental devices. In our proposed structure, in addition to providing a simple and fabricatable structure, the Al_2O_3 and other materials which have the lattice mismatch between the layers are not used.

To validate of the obtained simulation results, some of the structures which presented in other studies have been reproduced and scrutinized. The layers and interface defects have been analyzed based on the simulation confirmation of the structure by solar cell capacitance simulator (SCAPS). Then, in the first proposed structure, the p^+-CZTS ultrathin layer is introduced between the CZTS absorber layer and Mo back-contact. In the second suggested structure, p^+-CZTS/p-CZTS dual absorber layer is simulated to improve the photovoltaic parameters. In addition, the following sections are provided in this paper:

- Simulation of the baseline structure as Mo/CZTS/CdS/i-ZnO/ZnO:Al/Al solar cells and comprise with our structures.
- Investigating defects of layers and interfaces in the CZTS solar cell layers and simulation of their effects.
- Adding CZTS intermediate layer to increase photovoltaic parameters of solar cell.
- Using the dual layer p^+pn structure in CZTS-based thin film solar cells and optimization of the proposed structure to obtain the highest performance of the device.

2 Device structure

The baseline structure of kesterite solar cells is Mo/CZTS/CdS/i-ZnO/ZnO:Al/Al. Figure 1 depicts the main structure of the CZTS solar cell which grown on soda lime glass (SLG). CZTS and CdS are the absorber and buffer layers with band gap of 1.5 eV and 2.4 eV, respectively. As well, the intrinsic and n-doped layers of ZnO (i-ZnO and Al:ZnO) form window layers (Opanasyuk et al. 2012). Aluminum (Al) and molybdenum (Mo) are considered front and back contacts (Boutebakh et al. 2017). Flat band is automatically assigned to metal work function in the SCAPS, which is employed for the front-contact. However, a work function above 5 eV can be used for back-contact. The high-performance CZTS solar cells have the same basic structure. Some papers have tried to perform proper band offset in the absorber/buffer interface by changing the buffer layer (Burgelman et al. 2000; Wanda et al. 2019; Sinha et al. 2018). Nevertheless, first-principles calculations show that the band

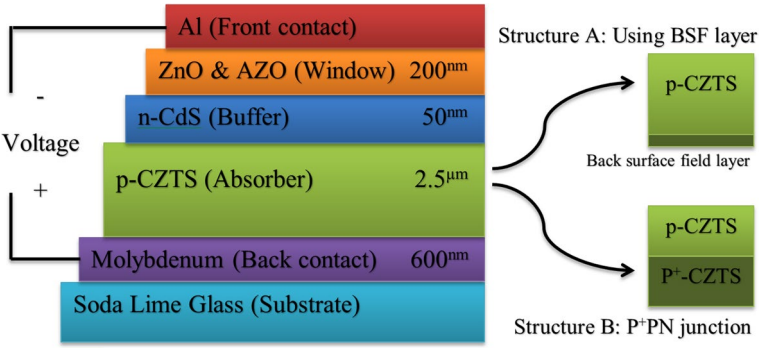

Fig. 1 Basic structure of CZTS-based thin film solar cell and two proposed structures; structure A with inserting p^+-CZTS intermediate layer and structure B dual layer with p^+pn junction

alignment of CZTS/CdS is cliff-type (Chen et al. 2011). Several studies confirm that conduction band offset (CBO) is formed cliff-type which enlarges the interface recombination. It acts as a block to prevent the flow of injected majority carriers (electrons) from the buffer layer to the absorber layer under forward bias (Sun et al. 2016). Nevertheless, all three types of "spike-type" (Shin et al. 2013; Park et al. 2015), "flat" (Tajima et al. 2013) and "cliff-type" (Ericson et al. 2013; Yan et al. 2014) have been reported in the literature. Different process conditions and/or measurement methods may be the cause of this discrepancy (Sun et al. 2016). Moreover, with a proper annealing (high temperature annealing following CdS deposition), cliff-type can be changed to spike-type which has the potential to improve the photovoltaic properties of CZTS cells (Yan et al. 2018). Consequently, the changing of the buffer layer is not necessary.

One of the reasons for the decline in open circuit voltage in kesterite solar cells is an enhancement in the carrier recombination at the interface of back-contact and CZTS. One of the key influential solutions which cause high open circuit voltage and efficiency in CIGS solar cells is the use of high p-doping near the back-contact and the gradual reduction of concentration to the absorber/buffer interface. This method is beneficial by making an electric field for the movement of minority carriers from the back-contact to the buffer layer and vice versa. Moreover, this solution helps to increase the solar cell efficiency through extending the effective diffusion length and deactivating the back-contact/absorber interface (making the contact ohmic) (Lundberg et al. 2005). The employment of this method has been also proposed for CZTSSe thin film solar cells (Mohammadnejad and Parashkouh 2017). However, it is not possible to fabricate such structures easily due to the presence of complexities and secondary phases in kesterite growth. Using other thin layers as back surface field (BSF) is another solution proposed for reducing recombination losses. Another suggested method for improving solar cell performance is the employment of only one layer with higher doping under the absorber layer. This approach, which has been also used in silicon solar cells, leads to a better transport of minority carriers from the bottom towards the depletion region (Narasinha and Rohatgi 1997; Khelifi et al. 2008). Furthermore, in a kesterite thin film solar cell, a change in the ratio of Cu/Sn and Zn/Sn is followed by an enlargement in the open circuit voltage (from 665 to 734 mV) (Yan et al. 2017). With the combination of the latter two methods in this work, the CZTS with a thickness of tens of nanometers and high doping is used under the absorber layer to improve the open circuit voltage and efficiency of the CZTS solar cell.

The two proposed structures are illustrated on the right side of Fig. 1; Structure A with inserting an ultrathin p^+-CZTS intermediate layer between Mo and CZTS absorber layer and structure B using dual layer with p^+pn junction. The thin layer in the structure A has a significant impact on improving the efficiency and open circuit voltage of the device. Additionally, the structure B uses a dual absorber layer to raise the efficiency and open circuit voltage.

3 Results and discussions

3.1 Verification of solar cell simulation

A comprehensive study has been performed on the performance of kesterite-based thin film solar cells in reference (Simya et al. 2015). To compare and validate the results of the present paper, the simulation results obtained from reference (Simya et al. 2015) are analyzed.

First, CZTS/CdS/ZnO structure is simulated and an efficiency of 8.97% obtained. Afterward, the impact of the series resistance, total recombination, defects, interface and various layers' thickness has been investigated. An efficiency of 12.03% is obtained by using the back-contact with a work function of 5.1 eV. The present study reproduced these results for validating the simulation as well as providing a detailed examination of the structure to enhance the performance of kesterite-based solar cells. Table 1 shows the conditions of simulation of CZTS solar cells. In addition, the properties of the absorber, buffer and window layers are shown in this table.

Table 2 presents the results obtained from the simulation of CZTS/CdS/ZnO structure with the efficiencies of 8.96% and 12.05%, respectively. Moreover, Table 2 demonstrates the photovoltaic parameters of these structures. It is possible to improve the solar cell performance from the voltage at maximum power (V_{MP}) to open circuit voltage to study the cause of curve bending in comparison with the ideal J–V curve under identical open circuit voltage (V_{OC}) and short-circuit current density (J_{SC}) conditions. Figure 2a, b illustrate the J–V curve reproduced from the conventional CZTS-based structure and the proposed structure of reference (Simya et al. 2015) in comparison with the ideal curve, respectively. The losses resulted by recombination currents including electron and hole minority carrier current, recombination in the body, recombination at the interface, Shockley-Reed-Hall recombination, radiative and Auger recombination are presented in Fig. 2c, d. The main reason for the improvement in the structure performance of Fig. 2b compared to Fig. 2a is the reduction in minority carrier current near the back-contact due to the employment of the back-contact with a work function of 5.1 eV higher than molybdenum's (5 eV). The notable decline in minority carrier recombination current from 13.93 to 5.31 mA/cm^2 and the reduction in interface recombination from 7.46 to 2.73 mA/cm^2 lead to the improvement in the performance of the CZTS/CdS/ZnO structure with the back-contact work function of 5.1 eV.

Interface recombination can be divided into three main groups: (1) cliff-type band alignment at the absorber/buffer interface, in a way that the conduction band edge of the buffer layer is lower than the absorber's and causes a recombination increase at the interface, (2) secondary phases in the interface by trapping minority charge carriers or creating shunt paths, (3) non-ohmic back-contact due to the formation of thick MoS_2 layer between CZTS and Mo contact, which enlarges series resistance (Gao et al. 2018). The interface recombination with the J–V curve of Fig. 2b is reduced by applying the back-contact with 5.1 eV work function. In fact, the higher work function of CZTS rather than that of molybdenum's leads to a high back-contact barrier (Φ_{bp}) which equals to 0.88 eV. It is possible to improve this state by replacing the back-contact and reducing Φ_{bp} to 0.78 eV.

The carrier recombination in the body and the high recombination rate at the absorber/buffer interface are considered as major reasons for the great deficit of V_{OC}. Body recombination results from extended band tail and deep intrinsic defects. As a result, there is higher non-radiative recombination and shorter lifetime of minority carriers in kesterite materials (Levcenko et al. 2016). Generally, in a p-type material with a small effective mass, such as kesterites, the radiative recombination is resulted by four different parts: (1) band-to-tail (BT) recombination, which is formed by a free electron and a hole in the band tail; (2) band-to-band (BB) recombination, which is brought about by a free electron and a free hole; (3) band-to-impurity (BI) recombination, which includes a deep acceptor that does not overlap with the band tail; (4) donor–acceptor pair (DAP) recombination, which consists of acceptor and donor states that are deep enough and do not overlap with the related band tails (Grossberg et al. 2019). The sum of these recombinations can be modeled as the radiative recombination coefficient (B_r),

Table 1 Condition and layer parameters in the simulation

Parameters (unit)	CZTS	CdS	i-ZnO	ZnO:Al	References
Band gap (eV)	1.50	2.40	3.30	3.30	Adewoyin et al. (2019)
Thickness (μm)	0–3	0.05	0.1	0.05	Adewoyin et al. (2019)
Electron affinity (eV)	4.25	4.20	4.45	4.45	Adewoyin et al. (2019)
Electron/hole mobility (cm^2/V s)	100/20	100/25	100/25	100/25	Mohammadnejad and Parashkouh (2017)
CB density of state (cm^{-3})	2.2×10^{18}	2.2×10^{18}	2.2×10^{18}	2.2×10^{18}	Seol et al. (2003)
VB density of state (cm^{-3})	1.8×10^{19}	1.8×10^{19}	1.8×10^{19}	1.8×10^{19}	Seol et al. (2003)
Dielectric permittivity	10	10	9	9	Mohammadnejad and Parashkouh (2017)
Electron/hole thermal velocity (cm/s)	1.0×10^{7}	1.0×10^{7}	1.0×10^{7}	1.0×10^{7}	Hossain et al. (2011)
Acceptor concentration (cm^{-3})	10^{15}–10^{18}	1×10^{2}	1×10^{1}	1×10^{1}	Hossain et al. (2011) and Wang et al. (2010)
Donor concentration (cm^{-3})	1×10^{3}	1×10^{17}	1×10^{15}	1×10^{18}	Khattak et al. (2018)
Absorption coefficient (cm^{-1})	5×10^{4}	SCAPS library	SCAPS library	SCAPS library	Burgelman et al. (2016)
Radiative recombination coefficient (cm^2/s)	1×10^{-9}	1×10^{-10}	1×10^{-10}	5×10^{-9}	Grossberg et al. (2019) and Adewoyin et al. 2017b)
Auger electron capture coefficient (cm^6/s)	10^{-28}	10^{-29}	10^{-28}	10^{-28}	
Auger hole capture coefficient (cm^6/s)	10^{-28}	10^{-29}	10^{-28}	10^{-28}	
Contacts	Back-contact		Front contact		
Metal work function (eV)	4.8–5.2		Flat band		
SRV of electron and hole (eV)	10^5, 10^7		10^7, 10^5		Burgelman et al. (2016)
Temperature (K)	300				–
Series resistance (Ω cm^2)	0.5–4				Redinger et al. (2013), Lin et al. (2014) and Simya et al. (2015)
Shunt resistance (Ω cm^2)	400–2000				Mohammadnejad and Parashkouh (2017) and Lin et al. (2014)

Table 2 Results obtained from the simulation of CZTS solar cell

Parameters	Structure 1		Structure 2	
	Existing Ref. (Simya et al. 2015)	Simulation (reproduced)	Existing Ref. (Simya et al. 2015)	Simulation (reproduced)
Eff. (%)	8.97	8.96	12.03	12.05
FF (%)	63.41	63.73	65.19	65.61
V_{OC} (mV)	640.7	628.3	744.7	731.4
J_{SC} (mA/cm^2)	22.07	22.38	24.79	25.09
V_{MP} (mV)	–	456.3	–	543.1
J_{MP} (mA/cm^2)	–	19.63	–	22.18

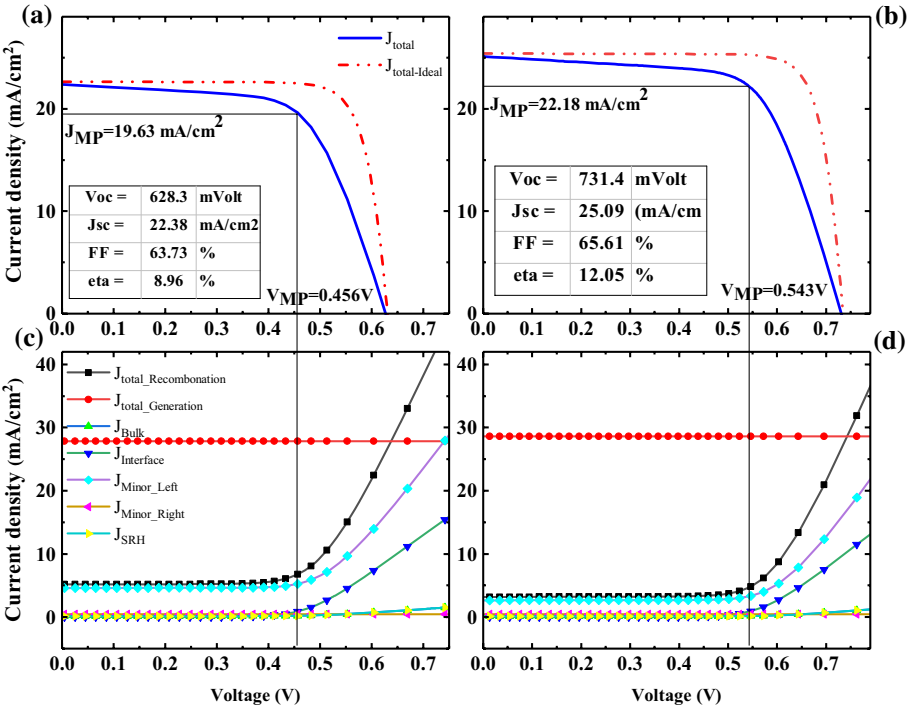

Fig. 2 J–V curve reproduced from **a** the conventional CZTS-based structure, **b** the proposed structure of reference (Simya et al. 2015) in comparison with the ideal curve; the generation and recombination current density in various regions related to **c** Fig. 2a, **d** Fig. 2b

which is about 10^{-11}–10^{-9} cm^3/s for a semiconductor with a direct band gap (Adewoyin et al. 2017b). This coefficient is 10^{-9} cm^3/s in the employed model and the simulation is eventually done by considering the electron and hole auger coefficient as 10^{-28} cm^6/s. The results of this analysis are shown in Table 3 and they are compared with the results of reference (Simya et al. 2015).

Table 3 Various generation and recombination current density values in the two structures of CZTS solar cell

Current density	0.6 V bias voltage (mA/cm^2)	
	Structure 1	Structure 2
J_{total}	4.42	19.44
$J_{total\text{-}generation}$	27.81	28.58
$J_{total\text{-}recombination}$	22.69	8.87
$J_{Minor\text{-}left}$	13.93	5.31
J_{Bulk}	0.70	0.27
$J_{Interface}$	7.46	2.73
J_{SRH}	0.74	0.27
$J_{Minor\text{-}right}$	0.43	0.43
$J_{Radiative}$	0.04	0.04
J_{Auger}	0.09	0.09

3.2 Defect modeling and simulation

Accurate analysis and simulation of CZTS-based structure are a great aid in designing and improving the performance of kesterite-based solar cell structures. The defects of absorber and buffer layers as well as those of absorber/buffer interface and buffer/window are used to obtain accurate results in the simulation. Point defects and clusters appear during the growth process of kesterite absorber layers. Gibbs free energy of the crystal is minimized during the growth process of kesterite absorber layer and forms vacancy, antisite and interstitial defects (Bourdais et al. 2016). The number of potential defects in the materials including 4 or 5 elements, such as kesterites is increased dramatically. Charge transition levels of point defects in the growth process of CZTS absorber layer are depicted and summarized in Fig. 3.

Generally, there are two types of concentrations in the kesterite: doping and alloying (Romanyuk et al. 2019). Many samples of CZTS are intrinsically p-type conductivities (Romanyuk et al. 2019). The p-type conduction depends on a large population of shallow defects such as the acceptor defects. Cu/(Zn + Sn) and Zn/Sn ratios can be changed by Cu vacancies (V_{Cu}) and Cu_{Zn} antisites (Romanyuk et al. 2019). Presence of secondary phases (e.g. Cu_2S or ZnS), deviation in cationic ratios of Cu/(Zn + Sn) and Zn/Sn, uncertainties of various measurement techniques and unwanted doping by elements such as Na from the glass substrate are effective in the impurity concentration of the kesterites (Romanyuk et al. 2019). Although ionization level of Cu_{Zn} is deeper than of V_{Cu}, high population produces a significant concentration of holes, and p-type conductivity of kesterite is usually intrinsic (Chen et al. 2013). Moreover, in stoichiometric samples of Cu_2ZnSnS_4, the Cu_{Zn} antisite is the dominant point defect (Chen et al. 2013). By reducing the Sn content of 11% (from 36 to 0.25%), the intrinsic doping can be changed over a wide range of 10^{15}–10^{18} cm^{-3} (Romanyuk et al. 2019; Haass et al. 2018).

Additionally, external doping of lighter alkali elements depends on the apparent carrier concentration with Sn content (Haass et al. 2018). Some of the most important devices involving extrinsic doping are reported (Giraldo et al. 2019). Na has been used in the literature for external doping of CZTS (Giraldo et al. 2019; Romanyuk et al. 2019). Prior to annealing, CZTS precursor samples are added to the solution containing these doping elements (Altamura et al. 2016). However, the reported hole concentrations from

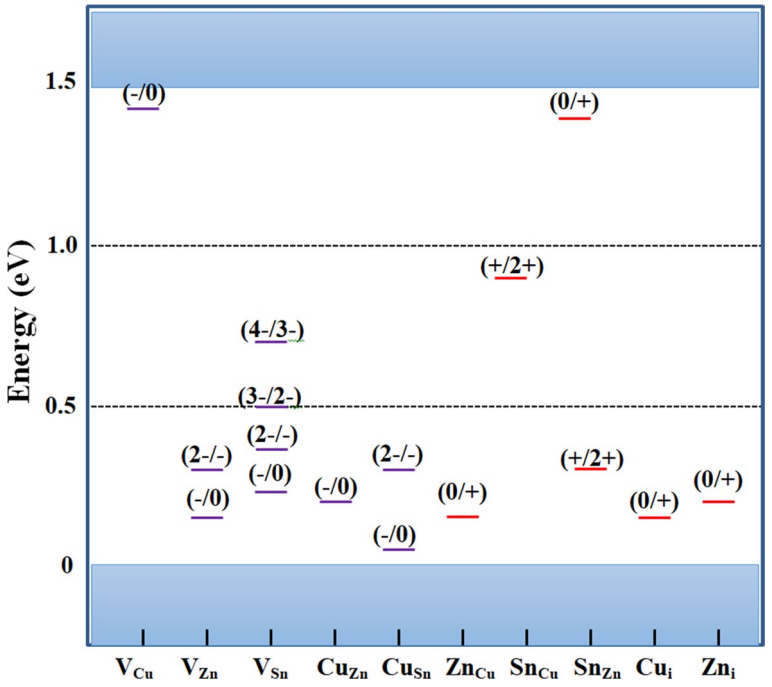

Fig. 3 Charge transition levels of vacancy (V_{Cu}, V_{Zn} and V_{Sn}), antisite (Cu_{Zn}, Cu_{Sn}, Zn_{Cu} and Sn_{Zn}) and interstitial (Cu_i and Zn_i) defects in Cu_2ZnSnS_4

various experiments covered the range from 1.2×10^{15} to 3.1×10^{20} cm^{-3} (Chen et al. 2013). Table 4 shows the various characteristics of defects in CZTS solar cell simulation.

In general, for silicon based solar cells, under normal operating conditions, the Shockley–Read–Hall (SHR) recombination mechanism predominates. Intra-bandgap transitions form defects and determine the performance of the device (Frazão et al. 2017). Although many progress has been made in describing and reducing light-induced degradation, industrial silicon solar cells still have a variety of defects (Lindroos and Savin 2016). These defects can be considered intrinsic or extrinsic. The intrinsic defect is because of the nature of the surface and interface recombination of the material, while the external defects are mainly due to the defects such as broken fingers and wafer cracks (Frazão et al. 2017). Nonetheless, the magnitude of defect density of silicon based solar cells is 10^{12} cm^{-2} (Limpens et al. 2016).

3.3 Optimizing the CZTS thin film solar cell performance

Investigating the defect and carrier concentration and reproducing the results of CZTS solar cells lead to an improvement in the device performance. As shown in Fig. 3, the energy of point defect formation in Cu_{Zn} is about 0.2 eV. Due to the low formation energy of this defect in comparison with other defects, kesterite materials are intrinsic p-type semiconductors (Levcenko et al. 2016). In CZTS growth techniques, Cu-poor and Zn-rich conditions are necessary for the expansion of stoichiometric single-phase crystals (Zhuk et al. 2017). In this way, the formation of secondary phases is prevented. This phenomenon

Table 4 Instrumental parameters in the kesterite solar cell

Parameters	P-CZTS	CdS	i-ZnO	ZnO:Al	CZTS/CdS interface	CdS/ZnO interface
Defect type	Donor and acceptor	Acceptor (–/0)	Acceptor (–/0)	Acceptor (–/0)	Neutral, donor and acceptor	Neutral
Total density (N_t)	1×10^{14} - 5×10^{14} cm^{-3}	1×10^{15} cm^{-3}	1×10^{10} cm^{-3}	1×10^{15} cm^{-3}	1×10^{10} 1×10^{12} cm^{-2}	1×10^{10} cm^{-2}
Capture cross section electrons and holes (cm^2)	5×10^{-13} 1×10^{-15}	1×10^{-15}	1×10^{-15}	3×10^{-15}	1×10^{-14} 5×10^{-15}	4×10^{-18}
Energetic distribution	Single	Gaussian	Gaussian	Gaussian	Uniform	Uniform
Energy level with respect to reference	0.1–0.4 eV, 0.05–0.3 eV	1.2 eV	1.2 eV	1.6 eV	0.5–0.6 eV	0.6–0.8 eV

causes an enhancement in V_{Cu} and Zn_{Cu-} point defects. In this state, the concentration of donor defects increases. Figure 4 shows the impact of changes in the concentration of CZTS defects on the output parameters of the kesterite thin film solar cell. An enlargement in the concentration of defects in CZTS reduces the diffusion lengths of electrons and holes through decreasing the minority carrier lifetime. Therefore, the solar cell performance decreases along with an elevation in the recombination losses of the photogenerated carriers. Nonetheless, the interesting point in Fig. 4 is that changes in the output parameters of CZTS solar cells do not always improve in an ascending way along with the growth in the majority carrier concentration. Specially, this phenomenon is depicted in V_{OC} and J_{SC} curves of Fig. 4c, d. In fact, with a greater increase in the majority carriers, the possibility of recombining carriers at the absorber/buffer interface increase and this leads to a reduction in the current and conversion efficiency. In other words, with an enlargement in the density of carriers to about 1×10^{17} cm^{-3}, the saturation process of the device elevates as well as V_{OC}. However, with a greater increase in the concentration of carriers, recombinations enlarge and the possibility of photogenerated electron accumulation is less. Photons with longer wavelengths and lower energy are absorbed in the depth of CZTS. Consequently, as the carrier concentration increases, the efficiency of the solar cell does not elevate. It has been concluded that the highest efficiency in the pure CZTS-based thin film solar cells is possible in the carrier concentration of 1×10^{16} cm^{-3}–1×10^{17} cm^{-3}. Furthermore, according to Fig. 4c, the carrier concentration of 1×10^{17} cm^{-3} is proposed for obtaining the highest open circuit voltage.

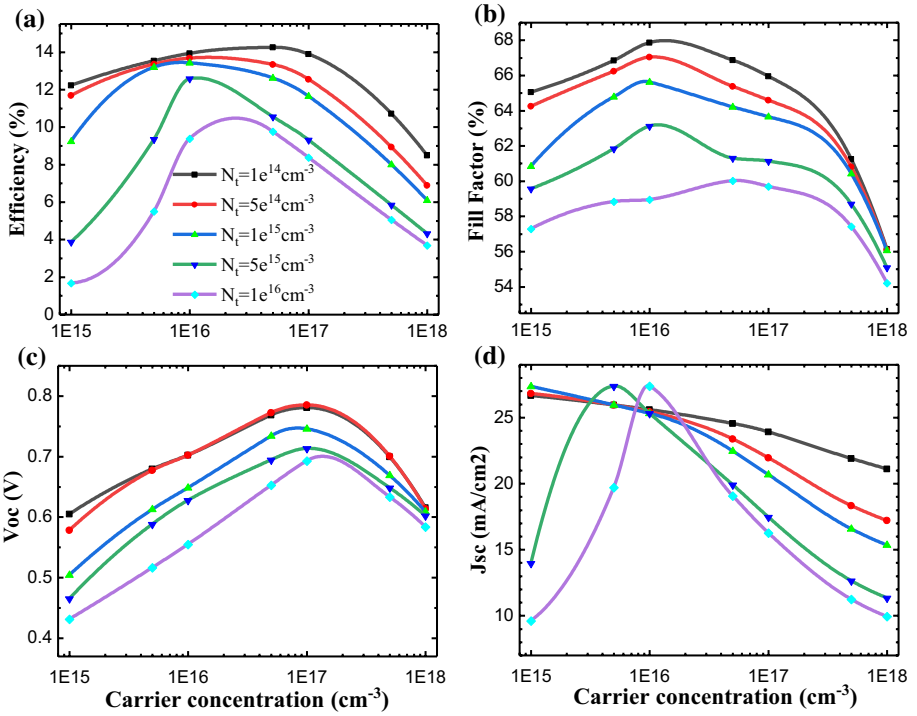

Fig. 4 **a** Efficiency, **b** fill factor, **c** V_{OC} and **d** J_{SC} of CZTS solar cells in various defect concentrations (N_t) as a function of carrier concentration

One of the methods proposed for increasing efficiency and open circuit voltage in kesterite solar cells is the use of alternative molybdenum as a back-contact. Despite the high work function of molybdenum (about 5 eV), one of the problems observed in chalcogenide solar cells is the combination of Mo with sulfur or selenium and the unintentional formation of $Mo(S,Se)_2$ thin layer. Similar to the CIGS structure, the formation of $MoSe_2$ interfacial layer causes an ohmic contact and helps to reduce the series resistance in CZTSe absorber layer (Marlein et al. 2009; Cozza et al. 2016). However, due to the low band gap of CZTSe, the solar cell which is based on this absorber layer has a lower open circuit voltage in comparison with CZTS. The MoS_2 interfacial layer, which is formed by the combination of Mo and S at the interface of molybdenum and CZTS, has been reported to be both n-type and p-type (Akdim et al. 2016). Even though it is shown in 2019 that the formation of MoS_2 with low electron affinity energy, a p-type impurity concentration above 1×10^{18} cm^{-3}, and a thickness of about tens of nanometers bring about a proper band alignment in the solar cell and increase its efficiency (Ferdaous et al. 2019). Most of the MoS_2 layers formed in CZTS solar cell structure are n-type and they cause a decrease in fill factor (FF) and efficiency as well as an enlargement in series resistance (R_S). (Akdim et al. 2016; Chelvanathan et al. 2018). There have been several attempts to solve this problem. Adding other thin layers such as SnS (Chen et al. 2016), Al_2O_3 (Liu et al. 2017), and ZnO (Li et al. 2014) help solve this problem. The employment of metals with proper work functions is one of the practical solutions.

As Fig. 5 demonstrates, in spite of the negative effects and formation of a new interfacial layer at the absorber/back-contact interface, the performance of CZTS based solar cell has been changed by variation of work function from 4.8 V to 5.2 V (Cozza et al. 2016). As the work function of back-contact increases, the barrier height in the valence band decrease and the photogenerated holes in the quasi-neutral region (QNR) move easier from the absorber layer to the back-contact. Therefore, holes recombination with input electrons from the external circuit is done at a higher rate and this enhances open circuit voltage and efficiency. This process is possible with metals such as Ni, Au, Pt, and Pd, which have a work function above 5 eV. If the optimal values of carrier concentration (1×10^{17} cm^{-3}) and the metal with a work function of 5.1 eV are employed in the back-contact, the solar cell efficiency increases to 12.43%.

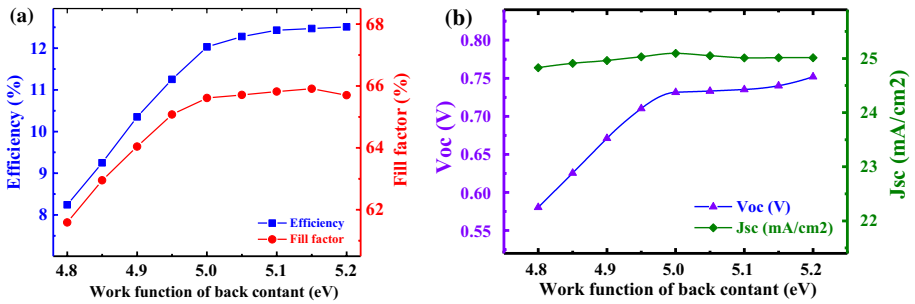

Fig. 5 Output parameters of the solar cells as a function of the alterations in back-contact work function, **a** efficiency and fill factor, **b** V_{OC} and J_{SC}

3.4 Introducing p^+-CZTS intermediate layer

The impact of the thickness of BSF thin layer on the output parameters of CZTS solar cell is shown in Fig. 6a. At the thickness of 50 nm, the solar cell efficiency increased to 14.43%. It is possible to enhance the efficiency of the solar cell (about 0.24%) by increasing the thickness from 50 nm to 300 nm. Due to the homogeneity of BSF and absorber layers, a further increase in the thickness of the BSF layer causes an enlargement in the CZTS layer. Nevertheless, this method contradicts the aims of the thin film solar cell and an enlargement in the thickness of the absorber layer through decreasing the series resistance which results in the reduction of open circuit voltage. Therefore, after choosing the optimum thickness of 200 nm, the solar cell efficiency enlarges to 14.59%. Moreover, the open circuit voltage in this structure is about 880 mV (FF = 66.81%, $J_{SC} = 24.82$ mA/cm^2). Once the optimum thickness of BSF thin layer is determined, it is expected that the solar cell performance improves along with the enlargement in carrier concentration. Figure 6b demonstrates the simulation results of the CZTS-based structure as a function of BSF carrier concentration. Accordingly, in the carrier concentration of 1×10^{18} cm^{-3}, the efficiency of this structure is 15.62% ($V_{OC} = 918$ mV, FF = 66.40%, $J_{SC} = 25/60$ mA/cm^2). In this structure, the concentration of the acceptor carriers in CZTS is selected to be 5×10^{16} cm^{-3} to obtain superior efficiency.

Under illumination, the charge carrier transport in the conventional solar cell is explained as follows: first, the photogenerated electrons in the quasi-neutral region (QNR) move from the CZTS absorber layer towards CZTS/CdS interface and then drift to the depletion region due to the built-in electric field and are eventually collected at the front electrodes. After that, the electrons collected by Mo contact return to the solar cell via an external circuit which is accompanied by energy dissipation. The photogenerated holes at the CZTS absorber layer move towards the back-contact and recombined with the incoming electrons from the external circuit. Insertion of the CZTS thin layer between the back-contact and CZTS change the charge carrier transport in the back-contact. The ohmic or Schottky junction between the back-contact and CZTS are effective in analysis of the current and recombination losses.

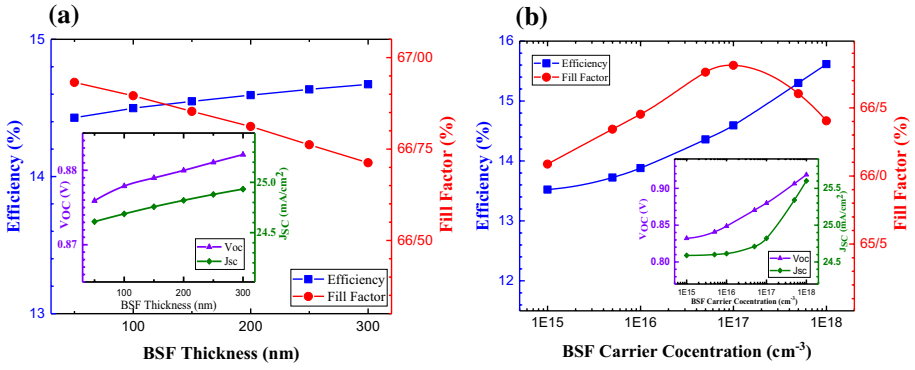

Fig. 6 **a** The thickness effect of BSF thin layer and **b** the impact of the BSF carrier concentration on the output parameters of CZTS solar cell. In part b, the thickness of BSF is 200 nm and the carrier concentration of the absorber layer is 5×10^{16} cm^{-3}

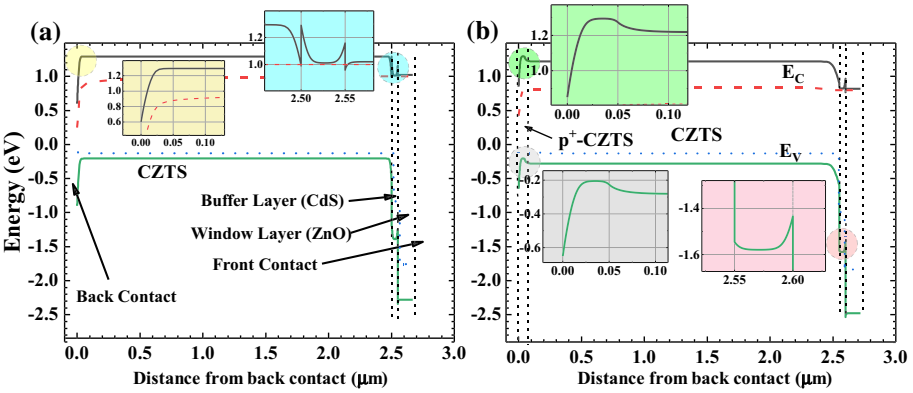

Fig. 7 Band diagram of conventional CZTS/CdS and p^+-CZTS/CZTS/CdS structures

Table 5 The band diagram parameters in p^+pn CZTS structures ($N_{A\text{-}(p\text{-}CZTS)}=5\times10^{15}$ cm^{-3} and $N_{A\text{-}(p+\text{-}CZTS)}=1\times10^{18}$ cm^{-3})

Band diagram parameters		p-CZTS	p^+-CZTS/p-CZTS
Mo/CZTS	Φ_{Bn} (eV)	0.72	0.950
	$\Phi_{Bp\text{-}}$ (eV)	0.78	0.550
	qV_o (eV)	0.434	0.456
p^+-CZTS/p-CZTS	ΔE_C (eV)	–	+ 0.020
	ΔE_V (eV)	–	− 0.030
	qV_{bi} (eV)	–	+ 0.143

Generally, the value of equilibrium contact potential (qV_o) is a barrier which prevents the transfer of holes from the absorber valence band (VB) to the back contact. The qV_o is the barrier for transport of electrons in CZTS/CdS absorber/buffer and CdS/ZnO buffer/window interfaces. In Schottky contacts, the amount of qV_o is greater than zero. The p^+-CZTS/p-CZTS and p-CZTS/n-CdS form the built-in voltage generated in back and front junction ($qV_{bi,back}$ and $qV_{bi,\ front}$), respectively. These built-in voltages are in the same polarities. Because of the relationship between the conduction band (Φ_{Bn}) and the valance band (Φ_{Bp}) as $\Phi_{Bn}+\Phi_{Bp}=E_{g,CZTS}$ within Mo/CZTS, only Φ_{Bp} is selected as the main parameter in determining the transport rate of the incoming electrons from the Mo Fermi level to the CZTS valence band.

Figure 7 demonstrates band diagram of conventional CZTS/CdS and p^+-CZTS/p-CZTS/n-CdS structures. The amount of conduction band offset (ΔE_C), valence band offset (ΔE_V), Φ_{Bn} and Φ_{Bp} are constant (see Table 5). Hence, the performance of the p^+-CZTS/CZTS/CdS solar cell depends only on qV_o and $qV_{bi,back}$. In general, the smaller the $qV_{bi,back}$ and qV_o, the better the transport of the hole from p^+-CZTS VB to Mo contact. As carrier concentration of BSF CZTS layer increases of higher qV_o and small negative values of qV_{bi} cause relatively good band bending in the CB and VB. The Fermi level moves downwards and the holes transfer faster from CZTS to p^+-CZTS. In addition, the electron current from CZTS to p^+-CZTS becomes lower and carrier recombination at the Mo/CZTS interface reduces. The insets of Fig. 7 show the band diagram magnification of CB and VB. The Φ_{Bp} of the Mo/CZTS interface in baseline structure is 0.78 eV. While

in Fig. 7b, this value has been reduced to 0.55 eV and has led to improvement in device performance. Besides, in Fig. 7b, changing of the CB and VB at the p^+-CZTS/p-CZTS interface have caused Φ_{Bp} to be 143 meV. This creates an electric field in the same direction with the V_{bi} at CZTS/CdS interface and increases the solar cell open circuit voltage. It also facilitates the separation of electrons and holes. Thus, improving of efficiency occurs by reducing recombination in the area near the back contact.

3.5 Using dual absorber layer

Despite the improvement of photovoltaic performance in the CZTS solar cell with a BSF layer of CZTS type, it is advisable to use a dual absorber layer with p^+p junction. As Fig. 8 shows, the device performance diminishes when the carrier concentration of upper CZTS decreases. But an optimized range is observed in the device output parameters when the downer CZTS absorber layer carrier concentration changes. Increasing the carrier concentration of the upper CZTS layer enhances the carrier recombination in the CZTS/CdS interface. Since the lower energy photons with longer wavelengths are absorbed in the deep of CZTS layers, the accumulation of photogenerated electrons decreases. Hence, J_{SC} and efficiency reduces. As a result, the highest V_{OC} of 939 mV and efficiency of 16.99% are obtained in dual absorber device. This performance occurs in carrier concentration of

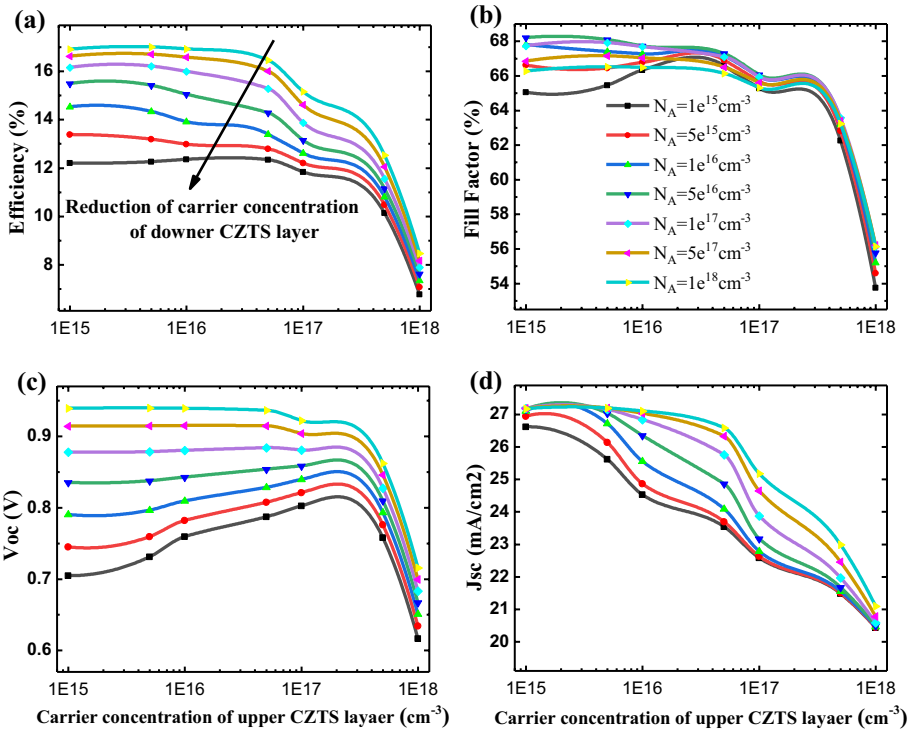

Fig. 8 Dual CZTS layer solar cell performance in the carrier concentration of the upper and downer CZTS layer

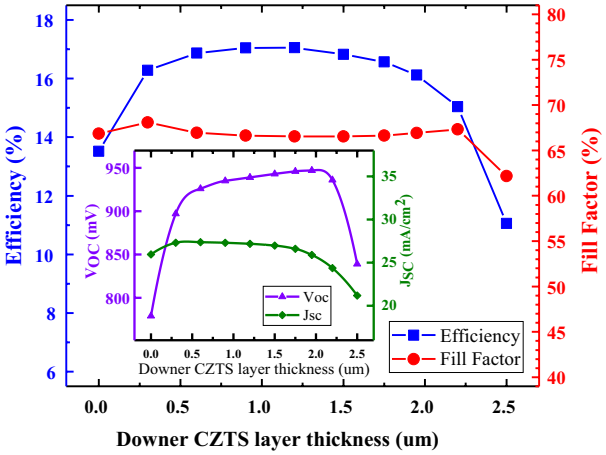

Fig. 9 Performance of dual CZTS layer solar cell with different ratio of upper/downer thickness

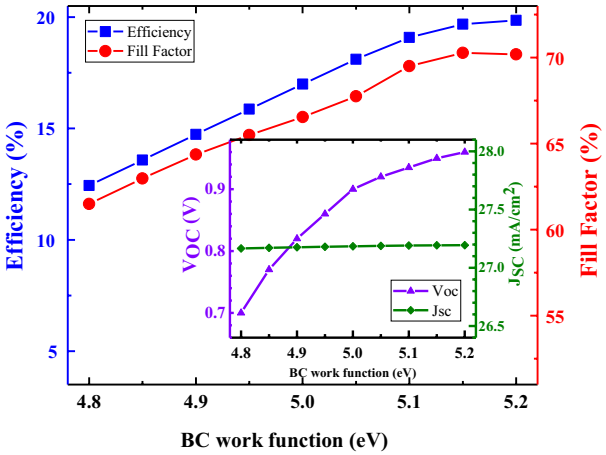

Fig. 10 Performance of dual CZTS layer solar cell versus back-contact work function

5×10^{15} cm^{-3} and 1×10^{18} cm^{-3} for upper and downer CZTS layers, respectively. Moreover, the J_{SC} and FF are 27.20 mA/cm^2 and 66.52%, respectively.

To provide a more accurate analysis of dual CZTS layer solar cell, the performance of this device at different thickness ratios of the dual absorber layer is presented in Fig. 9. The maximum efficiency is depicted in the thickness range of 800 to 1200 nm at the downer absorber layer. Furthermore, at the thickness of 1 µm, the solar cell efficiency equals to 17.05% and the open circuit voltage is about 941 mV ($J_{SC}=27.18$ mA/cm^2, FF = 66.54%).

One of the methods for improving the thin film solar cell efficiency is reducing the barrier height at the back-contact through increasing the back-contact to absorber layer work function. Figure 10 illustrates the efficiency, FF, V_{OC}, and J_{SC} curves for a change in work function. An efficiency of more than 16% is observed in the metals with a work function higher than 5.0 eV. Other metals with a range of 5 ± 0.2 eV can be used. Using the metals such as Pt, Pd or Au, enhances the efficiency more than 18%. The J-V curve of the dual absorber CZTS solar cell using p^+-CZTS/p-CZTS junction is depicted in Fig. 11. In this simulation, the carrier concentration of downer and upper absorber (p^+-CZTS and p-CZTS, respectively) layers are 1×10^{18} cm^{-3} and 5×10^{15} cm^{-3}, respectively. Furthermore, the

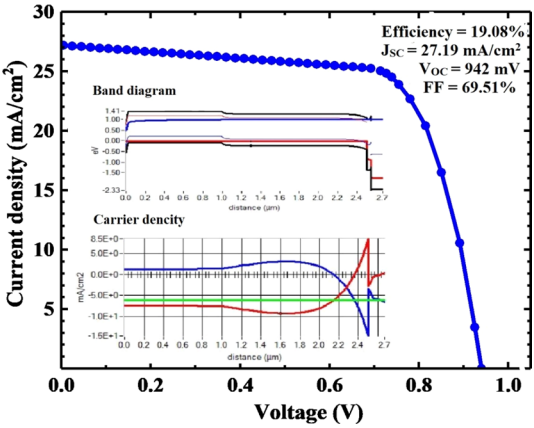

Fig. 11 The J–V curve of the dual absorber CZTS solar cell with the p^+pn structure by using p^+-CZTS/p-CZTS junction

thickness of above mentioned layers is 1 μm and 1.5 μm, respectively. Additionally, the band diagram of dual absorber layer structure and the current density of electrons and holes are demonstrated as insets of Fig. 11. No improvement is observed in the solar cell efficiency at higher thicknesses, which is due to the band structure at p^+-CZTS/p-CZTS interface. Band alignment at the interface of the p^+pn structure is presented in Fig. 11. The efficiency of this structure in 5.1 eV work function of back-contact is 19.08% (V_{OC} = 942 mV, FF = 69.51%, J_{SC} = 27.19 mA/cm^2).

Solar cell performance can also be considered from the J-V characteristic point of view. Figure 12 depicts the J–V curve of two optimized proposed structures (BSF/CZTS and p^+-CZTS/CZTS). The ideal curve (with the assumption of $R_s = 0$ and $R_{sh} = \infty$) of J-V has been drown for comparison of structures. The hatched area (in green) shows the range of V_{MP} difference of these characteristics. In the proposed structures, the recombination currents reached their minimum values and the highest open circuit voltage is obtained.

Table 6 shows the calculated values of current components at the bias voltage of 0.8 V. In the BSF/CZTS structure, despite the creation of back surface field by CZTS intermediate layer and the formation of MoS_2 at Mo/CZTS interface, the main recombination component is related to the interface and is equal to 5.84 mA/cm^2. In the dual absorber layer, the minority carrier recombination near the back-contact ($J_{Minnor\text{-}left}$) and the recombination of the carriers at the interface ($J_{Interface}$) are deduced as 3.45 mA/cm^2 and 5.73 mA/cm^2, respectively.

To improve the performance of p^+-CZTS/p-CZTS dual layer solar cell, a back-contact of 5.1 eV work function has been used and shows that the total recombination of carriers ($J_{total\text{-}Recombination}$) decreases from 7.40 mA/cm^2 to 2.05 mA/cm^2. In this structure, the recombination current density at the interface ($J_{Interface}$) reduces to 0.66 mA/cm^2. Consequently, the efficiency and V_{OC} enhance to 941 mV and 17.05%, respectively. Moreover, applying the back-contact with work function of 5.1 eV in dual absorber structure and formation appropriate p^+-CZTS/p-CZTS/n-CdS junction, the conversion efficiency reaches 19.08%. V_{OC}, J_{SC}, and FF are 942 mV, 27.19 mA/cm^2 and 69.51%, respectively.

Table 7 shows the simulation results obtained from the proposed structures in comparison with the reproduced results. In addition to optimizing the layers thickness and doping concentration, one of the methods used for optimizing the basic structure in reference (Simya et al. 2015) is modifying the back-contact with the 5.1 eV work function, which has obtained an efficiency of about 12%. The advantage of employing CZTS intermediate layer is an increase

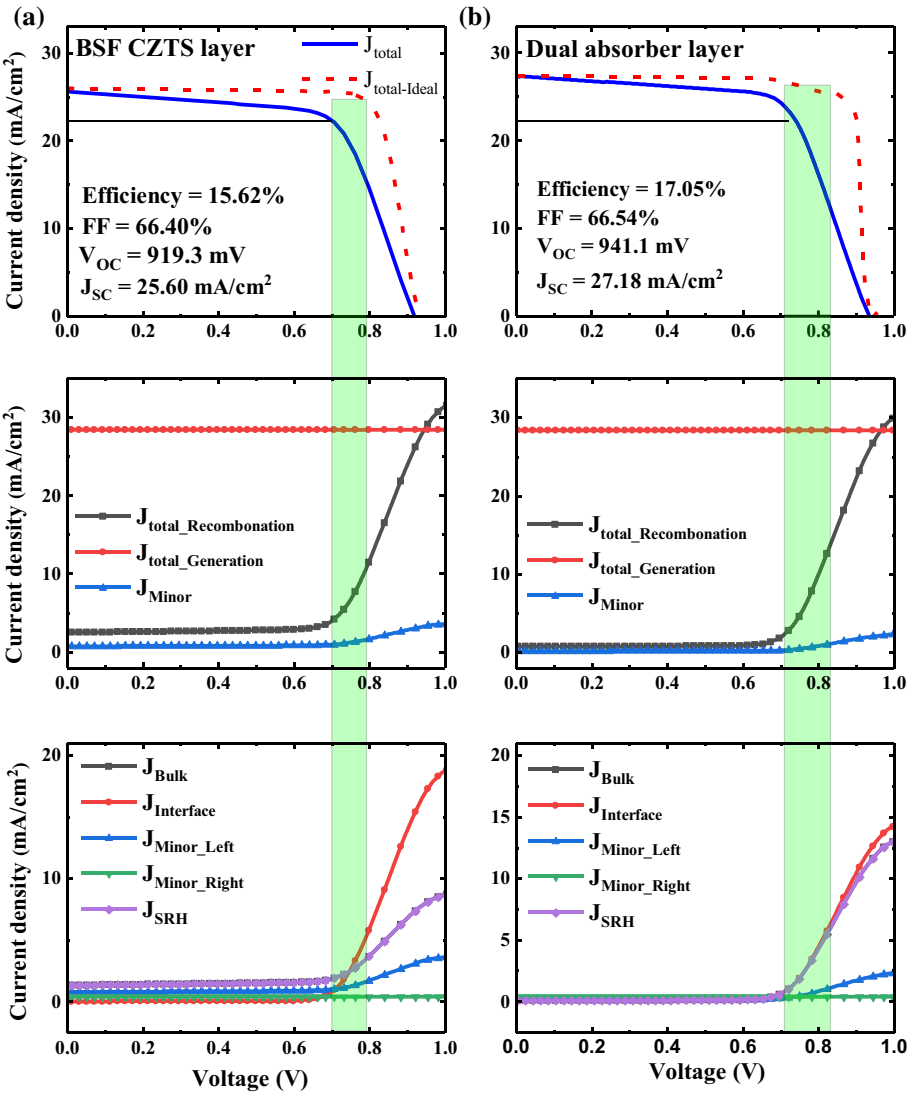

Fig. 12 J–V characteristics of the two optimized BSF/CZTS and p^+-CZTS/CZTS structures

in open circuit voltage and an improvement in CZTS-based solar cell efficiency. The efficiency of 14.25% is obtained from this structure and after optimizing the layers, the efficiency equaled 15.62%. Furthermore, with applying dual absorber layer as p^+-CZTS/p-CZTS and optimization this structure, 19.08% efficiency is achieved.

Table 6 Generation current density and recombination components of the proposed solar cells in comparison with reference (Simya, Mahaboobbatcha, and Balachander 2015). The values are calculated at 0.8-volt bias

Current density (mA/cm^2)	Baseline Structure		Proposed structures	
	Optimized (Simya et al. 2015)	Introducing intermediate CZTS	Dual absorber layer	Dual absorber layer (5.1 eV)
J_{total}	1.23	13.28	18.79	23.88
$J_{total\text{-}generation}$	28.58	28.44	28.35	28.41
$J_{total\text{-}recombination}$	38.32	11.71	7.40	2.05
$J_{Minor\text{-}left}$	22.86	1.68	5.73	3.17
J_{Bulk}	1.49	3.47	2.95	1.03
$J_{Interface}$	13.64	5.84	3.45	0.66
J_{SRH}	1.26	3.64	2.94	0.65
$J_{Minor\text{-}right}$	0.43	0.42	0.43	0.42
$J_{Radiative}$	0.04	0.04	0.04	0.04
J_{Auger}	0.09	0.09	0.09	0.09

Table 7 The simulation results obtained from the proposed structures in comparison with the reproduced results

Structure (CZTS/CdS)		Eff. (%)	FF (%)	V_{OC} (V)	J_{SC} (mA/cm^2)
Baseline	Reproduced (Simya et al. 2015)	8.96	63.73	628.3	22.38
	Optimized (Simya et al. 2015) (reproduced)	12.05	65.61	731.4	25.09
	Optimized (this work)	12.43	65.82	735.2	25.01
CZTS intermediate layer	This work	14.25	66.86	768.1	24.54
	Optimized (this work)	15.62	66.40	919.3	25.60
Dual absorber layer	p^+pn structure (this work)	17.05	66.54	941.1	27.18
	Optimized (this work)	19.08	69.51	942.3	27.19

4 Conclusion

In this paper, practical designs have been provided to overcome the low efficiency and V_{OC} deficit in CZTS based solar cells by two proposing practical structures, inserting p^+-CZTS ultrathin layer between Mo and p-CZTS layer, and using dual absorber layer. The effect of various layers and interface parameters such as thickness, carrier concentration, defect density and current recombination are studied, carefully. First, the results of the structure with 12.03% efficiency are reproduced to verify the validity of the simulation. The analysis demonstrates that it is possible to obtain an efficiency of 12.43% through changing the carrier concentration of CZTS absorber layer with considering its defects. In continue, it is shown that it is possible to increase the efficiency and open circuit voltage of kesterite solar cell to respectively 15.62% and 919 mV through inserting CZTS as a BSF layer with a thickness of 200 nm and carrier concentration of 1×10^{18} cm^{-3}. Moreover, dual CZTS absorber layer with p^+pn structure is proposed to enhance the photovoltaic parameters. In this dual absorber-based structure, the device conversion efficiency increases to 17.05% by selecting

the thickness of 1 μm and the carrier concentration of 1×10^{18} cm^{-3} for the p^+-CZTS layer and choosing the carrier concentration of 5×10^{15} cm^{-3} for the p-CZTS. In addition, the efficiency of this structure with 5.1 eV work function of back-contact is 19.08%.

References

Adewoyin, A.D., Olopade, M.A., Chendo, M.: Prediction and optimization of the performance characteristics of CZTS thin film solar cell using band gap grading. Opt. Quant. Electron. **49**, 336 (2017a)

Adewoyin, A.D., Olopade, M.A., Chendo, M.: Enhancement of the conversion efficiency of Cu_2ZnSnS_4 thin film solar cell through the optimization of some device parameters. Optik **133**, 122–131 (2017b)

Adewoyin, A.D., Olopade, M.A., Oyebola, O.O., Chendo, M.A.: Development of CZTGS/CZTS tandem thin film solar cell using SCAPS-1D. Optik **176**, 132–142 (2019)

Akdim, B., Pachter, R., Mou, S.: Theoretical analysis of the combined effects of sulfur vacancies and analyte adsorption on the electronic properties of single-layer MoS2. Nanotechnology **27**, 185701 (2016)

Altamura, G., Wang, M., Choy,-L.: Influence of alkali metals (Na, Li, Rb) on the performance of electrostatic spray-assisted vapor deposited Cu 2 ZnSn (S, Se) 4 solar cells. Sci. Rep. **6**, 22109 (2016)

Bahrami, A., Mohammadnejad, S., Soleimaninezhad, S.: Photovoltaic cells technology: principles and recent developments. Opt. Quant. Electron. **45**, 161–197 (2013)

Bourdais, S., Choné, C., Delatouche, B., Jacob, A., Larramona, G., Moisan, C., Lafond, A., Donatini, F., Rey, G., Siebentritt, S.: Is the Cu/Zn disorder the main culprit for the voltage deficit in kesterite solar cells? Adv. Energy Mater. **6**, 1502276 (2016)

Boutebakh, F.Z., Lamri Zeggar, M., Attaf, N., Aida, M.S.: Electrical properties and back contact study of CZTS/ZnS heterojunction. Optik **144**, 180–190 (2017)

Burgelman, M., Nollet, P., Degrave, S.: Modelling polycrystalline semiconductor solar cells. Thin Solid Films **361**, 527–532 (2000)

Burgelman, M., Koen, D., Alex, N., Johan, V., Stefaan, D.: SCAPS manual. In: February (2016)

Chelvanathan, P., Shahahmadi, S.A., Ferdaous, M.T., Sapeli, M.M.I., Sopian, K., Amin, N.: Controllable formation of MoS2 via preferred crystallographic orientation modulation of DC-sputtered Mo thin film. Mater. Lett. **219**, 174–177 (2018)

Chen, S., Walsh, A., Yang, J.-H., Gong, X.-G., Sun, L., Yang, P.-X., Chu, J.-H., Wei, S.-H.: Compositional dependence of structural and electronic properties of Cu_2ZnSn (S, Se) 4 alloys for thin film solar cells. Phys. Rev. B **83**, 125201 (2011)

Chen, S., Walsh, A., Gong, X.-G., Wei, S.-H.: Classification of lattice defects in the kesterite Cu_2ZnSnS_4 and $Cu_2ZnSnSe_4$ earth-abundant solar cell absorbers. Adv. Mater. **25**, 1522–1539 (2013)

Chen, H.-J., Sheng-Wen, F., Shih-Hsiung, W., Tsai, T.-C., Hsuan-Ta, W., Shih, C.-F.: Impact of SnS buffer layer at Mo/Cu_2ZnSnS_4 interface. J. Am. Ceram. Soc. **99**, 1808–1814 (2016)

Cherouana, A., Labbani, R.: Study of CZTS and CZTSSe solar cells for buffer layers selection. Appl. Surf. Sci. **424**, 251–255 (2017)

Cozza, D., Ruiz, C.M., Duché, D., Simon, J.J., Escoubas, L.: Modeling the back contact of $Cu_2ZnSnSe_4$ solar cells. IEEE J. Photovolt. **6**, 1292–1297 (2016)

Crovetto, A., Hansen, O.: What is the band alignment of Cu_2ZnSn (S, $Se)_4$ solar cells? Sol. Energy Mater. Sol. Cells **169**, 177–194 (2017)

Degen, S., Krupski, A., Kralj, M., Langner, A., Becker, C., Sokolowski, M., Wandelt, K.: Determination of the coincidence lattice of an ultra thin Al_2O_3 film on Ni_3Al (1 1 1). Surf. Sci. **576**, L57–L64 (2005)

Dey, M., Dey, M., Rahman, N., Tasnim, I., Chakma, R., Aimon, U., Matin, M.A., Amin, N.: Numerical modeling of SnS ultra-thin solar cells. In: 2017 International Conference on Electrical, Computer and Communication Engineering (ECCE), 911-15. IEEE (2017)

Ericson, T., Scragg, J.J., Hultqvist, A., Wätjen, J.T., Szaniawski, P., Törndahl, T., Platzer-Björkman, C.: Zn (O, S) Buffer layers and thickness variations of CdS buffer for Cu_2ZnSnS_4 solar cells. IEEE J. Photovolt. **4**, 465–469 (2013)

Ferdaous, M.T., Shahahmadi, S.A., Chelvanathan, P., Md Akhtaruzzaman, F.H., Alharbi, K.S., Tiong, S.K., Amin, N.: Elucidating the role of interfacial MoS2 layer in Cu_2ZnSnS_4 thin film solar cells by numerical analysis. Sol. Energy **178**, 162–172 (2019)

Frazão, M., Silva, J.A., Lobato, K., Serra, J.M.: Electroluminescence of silicon solar cells using a consumer grade digital camera. Measurement **99**, 7–12 (2017)

Gao, S., Jiang, Z., Li, W., Jianping Ao, Yu., Zeng, Y.S., Zhang, Y.: Interfaces of high-efficiency kesterite Cu_2ZnSnS $(e)_4$ thin film solar cells. Chin. Phys. B **27**, 018803 (2018)

Giraldo, S., Jehl, Z., Placidi, M., Izquierdo-Roca, V., Pérez-Rodríguez, A., Saucedo, E.: Progress and perspectives of thin film kesterite photovoltaic technology: a critical review. Adv. Mater. **31**, 1806692 (2019)

Green, M.A., Dunlop E.D., Levi, D.H., Hohl-Ebinger, J., Yoshita, M., Ho-Baillie, A.W.Y.: Solar cell efficiency tables (version 54). In: Progress in Photovoltaics: Research and Applications, p. 27 (2019)

Grossberg, M., Krustok, J., Hages, C.J., Bishop, D., Gunawan, O., Scheer, R., Lyam, S.M., Hempel, H., Levcenko, S., Unold, T.: The electrical and optical properties of kesterites. J. Phys. Energy **21**, 044002 (2019)

Guo, H., Ma, C., Zhang, K., Jia, X., Li, Y., Yuan, N., Ding, J.: The fabrication of Cd-free Cu_2ZnSnS_4-Ag_2ZnSnS_4 heterojunction photovoltaic devices. Sol. Energy Mater. Sol. Cells **178**, 146–153 (2018)

Haass, S.G., Andres, C., Figi, R., Schreiner, C., Bürki, M., Romanyuk, Y.E., Tiwari, A.N.: Complex interplay between absorber composition and alkali doping in high-efficiency kesterite solar cells. Adv. Energy Mater. **8**, 1701760 (2018)

Hossain, M.I.: Prospecs of CZTS solar cells from the perspective of material properties, fabrication methods and current research challenges. Chalcogenide Lett. **9**, 231–242 (2012)

Hossain, M.I., Chelvanathan, P., Mukter Zaman, M.R., Karim, M.A., Amin, N.: Prospects of indium sulphide as an alternative to cadmium sulphide buffer layer in CIS based solar cells from numerical analysis. Chalcog. Lett. **8**, 315–324 (2011)

Khattak, Y.H., Baig, F., Toura, H., Ullah, S., Marí, B., Beg, S., Ullah, H.: Effect of CZTSe BSF and minority carrier life time on the efficiency enhancement of CZTS kesterite solar cell. Curr. Appl. Phys. **18**, 633–641 (2018)

Khelifi, S., Verschraegen, J., Burgelman, M., Belghachi, A.: Numerical simulation of the impurity photovoltaic effect in silicon solar cells. Renew. Energy **33**, 293–298 (2008)

Khoshsirat, N., Yunus, N.A.: Numerical analysis of In2S3 layer thickness, band gap and doping density for effective performance of a CIGS solar cell using SCAPS. J. Electron. Mater. **45**, 5721–5727 (2016)

Levcenko, S., Just, J., Alex Redinger, G., Larramona, S.B., Dennler, G., Jacob, A., Unold, T.: Deep defects in $Cu_2ZnSn(S, Se)_4$ solar cells with varying Se content. Phys. Rev. Appl. **5**, 024004 (2016)

Li, W., Chen, J., Cui, H., Liu, F., Hao, X.: Inhibiting MoS_2 formation by introducing a ZnO intermediate layer for Cu2ZnSnS4 solar cells. Mater. Lett. **130**, 87–90 (2014)

Limpens, R., Luxembourg, S.L., Weeber, A.W., Gregorkiewicz, T.: Emission efficiency limit of Si nanocrystals. Sci. Rep. **6**, 19566 (2016)

Lin, P., Lin, L., Jinling, Yu., Cheng, S., Peimin, L., Zheng, Q.: Numerical simulation of Cu_2ZnSnS_4 based solar cells with In2S3 buffer layers by SCAPS-1D. J. Appl. Sci. Eng. **17**, 383–390 (2014)

Lindroos, J., Savin, H.: Review of light-induced degradation in crystalline silicon solar cells. Sol. Energy Mater. Sol. Cells **147**, 115–126 (2016)

Liu, Fangyang, Huang, Jialiang, Sun, Kaiwen, Yan, Chang, Shen, Yansong, Park, Jongsung, Aobo, Pu, Zhou, Fangzhou, Xu, Liu, Stride, J.A.: Beyond 8% ultrathin kesterite Cu_2 $ZnSnS_4$ solar cells by interface reaction route controlling and self-organized nanopattern at the back contact. NPG Asia Mater **9**, e401 (2017)

Lundberg, O., Edoff, M., Stolt, L.: The effect of Ga-grading in CIGS thin film solar cells. Thin Solid Films **480**, 520–525 (2005)

Maklavani, S.E., Mohammadnejad, S.: Enhancing the open-circuit voltage and efficiency of CZTS thin-film solar cells via band-offset engineering. Opt. Quant. Electron. **52**, 72 (2020)

Marlein, J., Decock, K., Burgelman, M.: Analysis of electrical properties of CIGSSe and Cd-free buffer CIGSSe solar cells. Thin Solid Films **517**, 2353–2356 (2009)

Miller, D.W., Warren, C.W., Gunawan, O., Gokmen, T., Mitzi, D.B., Cohen, J.D.: Electronically active defects in the Cu_2ZnSn $(Se, S)_4$ alloys as revealed by transient photocapacitance spectroscopy. Appl. Phys. Lett. **101**, 142106 (2012)

Mohammadnejad, S., Parashkouh, A.B.: CZTSSe solar cell efficiency improvement using a new band-gap grading model in absorber layer. Appl. Phys. A **123**, 758 (2017)

Nagaoka, A., Yoshino, K., Aoyagi, K., Minemoto, T., Nose, Y., Taniyama, T., Kakimoto, K., Miyake, H.: Thermo-physical properties of Cu_2ZnSnS_4 single crystal. J. Cryst. Growth **393**, 167–170 (2014)

Nakamura, Motoshi, Yamaguchi, Koji, Kimoto, Yoshinori, Yasaki, Yusuke, Kato, Takuya, Sugimoto, Hiroki: Cd-free Cu (In, Ga)$(Se, S)_2$ thin-film solar cell with record efficiency of 23.35%. IEEE J. Photovolt. **5**, 1863–1867 (2019)

Narasinha, S., Rohatgi, A.: Optimized aluminum back surface field techniques for silicon solar cells. In: Conference Record of the Twenty Sixth IEEE Photovoltaic Specialists Conference, pp. 63–66. IEEE (1997)

Neuschitzer, M., Lienau, K., Guc, M., Barrio, L.C., Haass, S., Prieto, J.M., Sanchez, Y., Espindola-Rodriguez, M., Romanyuk, Y., Perez-Rodriguez, A.: Towards high performance Cd-free CZTSe solar cells with a ZnS (O, OH) buffer layer: the influence of thiourea concentration on chemical bath deposition. J. Phys. D Appl. Phys. **49**, 125602 (2016)

Opanasyuk, A.S., Kurbatov, D.I., Ivashchenko, M.M., Yu Protsenko, I., Cheong, H.: Properties of the window layers for the CZTSe and CZTS based solar cells. J. Nano- Electron. Phys. **4**, 1024-1 (2012)

Pal, K., Singh, P., Bhaduri, A., Thapa, K.B.: Current challenges and future prospects for a highly efficient (> 20%) kesterite CZTS solar cell: a review. Sol. Energy Mater. Sol. Cells **196**, 138–156 (2019)

Pandey, S.K., Mukherjee, S.: Device modeling and optimization of high-performance thin film CIGS solar cell with Mg_xZn_{1-x} O buffer layer. In: 2013 IEEE 5th International on Nanoelectronics Conference (INEC), pp. 353–56. IEEE (2013)

Park, H.H., Heasley, R., Sun, L., Steinmann, V., Jaramillo, R., Hartman, K., Chakraborty, R., Sinsermsuksakul, P., Chua, D., Buonassisi, T.: Co-optimization of SnS absorber and Zn (O, S) buffer materials for improved solar cells. Prog. Photovolt. Res. Appl. **23**, 901–908 (2015)

Patel, M., Ray, A.: Enhancement of output performance of Cu_2ZnSnS_4 thin film solar cells—a numerical simulation approach and comparison to experiments. Physica B **407**, 4391–4397 (2012)

Pawar, B.S., Pawar, S.M., Shin, S.W., Choi, D.S., Park, C.J., Kolekar, S.S., Kim, J.H.: Effect of complexing agent on the properties of electrochemically deposited Cu_2ZnSnS_4 (CZTS) thin films. Appl. Surf. Sci. **257**, 1786–1791 (2010)

Ramanujam, J., Amit Verma, B., González-Díaz, R.G.-L., del Cañizo, C., García-Tabarés, E., Rey-Stolle, I., Granek, F., Korte, L., Tucci, M.: Inorganic photovoltaics—planar and nanostructured devices. Prog. Mater Sci. **82**, 294–404 (2016)

Redinger, A., Mousel, M., Wolter, M.H., Valle, N., Siebentritt, S.: Influence of S/Se ratio on series resistance and on dominant recombination pathway in $Cu_2ZnSn\ (SSe)_4$ thin film solar cells. Thin Solid Films **535**, 291–295 (2013)

Rizi, M.T., Shahrokh Abadi, M.H., Ghaneii, M.: Two dimensional modeling of Cu_2O heterojunction solar cells based-on β-Ga_2O_3 buffer. Optik **155**, 121–132 (2018)

Romanyuk, Y.E., Haass, S.G., Giraldo, S., Placidi, M., Tiwari, D., Fermin, D.J., Hao, X., Xin, H., Schnabel, T., Kauk-Kuusik, M.: Doping and alloying of kesterites. J. Phys. Energy **1**, 044004 (2019)

Scragg, J.J., Tomas Kubart, J., Wätjen, T., Ericson, T., Linnarsson, M.K., Platzer-Björkman, C.: Effects of back contact instability on Cu_2ZnSnS_4 devices and processes. Chem. Mater. **25**, 3162–3171 (2013)

Seol, J.-S., Lee, S.-Y., Lee, J.-C., Nam, H.-D., Kim, K.-H.: Electrical and optical properties of Cu_2ZnSnS_4 thin films prepared by rf magnetron sputtering process. Sol. Energy Mater. Sol. Cells **75**, 155–162 (2003)

Shin, B., Gunawan, O., Zhu, Y., Bojarczuk, N.A., Chey, S.J., Guha, S.: Thin film solar cell with 8.4% power conversion efficiency using an earth-abundant Cu_2ZnSnS_4 absorber. Progr Photovolt Res Appl **21**, 72–76 (2013)

Shin, D., Saparov, B., Mitzi, D.B.: Defect engineering in multinary earth-abundant chalcogenide photovoltaic materials. Adv. Energy Mater. **7**, 1602366 (2017)

Siebentritt, S.: Why are kesterite solar cells not 20% efficient? Thin Solid Films **535**, 1–4 (2013)

Simya, O.K., Mahaboobbatcha, A., Balachander, K.: A comparative study on the performance of Kesterite based thin film solar cells using SCAPS simulation program. Superlattices Microstruct. **82**, 248–261 (2015)

Sinha, S., Nandi, D.K., Kim, S.-H., Heo, J.: Atomic-layer-deposited buffer layers for thin film solar cells using earth-abundant absorber materials: a review. Sol. Energy Mater. Sol. Cells **176**, 49–68 (2018)

Sun, K., Yan, C., Liu, F., Huang, J., Zhou, F., Stride, J.A., Green, M., Hao, X.: Over 9% efficient kesterite Cu2ZnSnS4 solar cell fabricated by using Zn1–xCdxS buffer layer. Adv. Energy Mater. **6**, 1600046 (2016)

Tajima, S., Kataoka, K., Takahashi, N., Kimoto, Y., Fukano, T., Hasegawa, M., Hazama, H.: Direct measurement of band offset at the interface between CdS and Cu2ZnSnS4 using hard X-ray photoelectron spectroscopy. Appl. Phys. Lett. **103**, 243906 (2013)

Wanda, M.D., Ouédraogo, S., Ndjaka, J.M.B.: Theoretical analysis of minority carrier lifetime and Cd-free buffer layers on the CZTS based solar cell performances. Optik **183**, 284–293 (2019)

Wang, K., Gunawan, O., Todorov, T., Shin, B., Chey, S.J., Bojarczuk, N.A., Mitzi, D., Guha, S.: Thermally evaporated Cu_2ZnSnS_4 solar cells. Appl. Phys. Lett. **97**, 143508 (2010)

Wang, W., Winkler, M.T., Gunawan, O., Gokmen, T., Todorov, T.K., Zhu, Y., Mitzi, D.B.: Device characteristics of CZTSSe thin-film solar cells with efficiency. Adv. Energy Mater. **4**, 1301465 (2014)

Yan, C., Liu, F., Song, N., Ng, B.K., Stride, J.A., Tadich, A., Hao, X.: Band alignments of different buffer layers (CdS, Zn (O, S), and In_2S_3) on Cu_2ZnSnS_4. Appl. Phys. Lett. **104**, 173901 (2014)

Yan, C., Liu, F., Sun, K., Song, N., Stride, J.A., Zhou, F., Hao, X., Green, M.: Boosting the efficiency of pure sulfide CZTS solar cells using the In/Cd-based hybrid buffers. Sol. Energy Mater. Sol. Cells **144**, 700–706 (2016)

Yan, C., Sun, K., Liu, F., Huang, J., Zhou, F., Hao, X.: Boost Voc of pure sulfide kesterite solar cell via a double CZTS layer stacks. Sol. Energy Mater. Sol. Cells **160**, 7–11 (2017)

Yan, C., Huang, J., Sun, K., Johnston, S., Zhang, Y., Sun, H., Aobo, P., He, M., Liu, F., Eder, K.: Cu_2ZnSnS_4 solar cells with over 10% power conversion efficiency enabled by heterojunction heat treatment. Nat. Energy **3**, 764 (2018)

Yang, K.-J., Son, D.-H., Sung, S.-J., Sim, J.-H., Kim, Y.-I., Park, S.-N., Jeon, D.-H., Kim, J., Hwang, D.-K., Jeon, C.-W.: A band-gap-graded CZTSSe solar cell with 12.3% efficiency. J. Mater. Chem. A **4**, 10151–10158 (2016)

Zhuk, S., Kushwaha, A., Wong, T.K., Masudy-Panah, S., Smirnov, A., Dalapati, G.K.: Critical review on sputter-deposited Cu2ZnSnS4 (CZTS) based thin film photovoltaic technology focusing on device architecture and absorber quality on the solar cells performance. Sol. Energy Mater. Sol. Cells **171**, 239–252 (2017)